A&A 365, 268–274 (2001)
DOI: 10.1051/0004-6361:20000032
© ESO 2001

Astronomy & Astrophysics

Atomic data from the Iron Project

XLVII. Electron impact excitation of Ni III*

M. A. Bautista

Laboratory for High Energy Astrophysics, Code 662, NASA Goddard Space Flight Center, Greenbelt, MD 20771, USA

Received 29 August 2000 / Accepted 17 October 2000

Abstract. This paper reports R-matrix calculations of electron impact excitation rates for Ni III. The calculation includes 70 *LS* terms corresponding to the configurations $3d^8$, $3d^7 4s$, $3d^7 4p$, and $3d^6 4s^2$. This expansion results in 162 fine structure levels and 13 041 transitions, including optical, infrared, and ultraviolet lines. The collision strengths, including detailed resonance structures, were integrated over a Maxwellian distribution of electron energies and the resulting effective collision strengths are given for a wide range of temperatures. A collisional-radiative equilibrium model of the Ni III ion is constructed and the strongest lines in the optical and infrared spectral regions are identified. The emissivities of these lines and emissivity line ratio diagnostics are presented.

Key words. atomic data – line: formation – ISM: abundances – ultraviolet: general

1. Introduction

Forbidden Ni III lines are commonly detected in deep optical spectra of gaseous nebulae. These lines together with those of Ni II and Ni IV could be used for reliable estimates of the gas phase nickel abundance in nebulae. However, detailed calculations of collisional excitation rates have never been reported, so most abundance estimates rely entirely on [Ni II] emission. Such estimates have proven unreliable as they have led to abnormally high and variable Ni/Fe abundance ratios. This problem is known as the nickel-to-iron problem (Henry & Fesen 1988; Oliva et al. 1988; Haas et al. 1996) which has long lasted in the context of H II regions (e.g. Grandi 1975; Osterbrock et al. 1992; Bautista et al. 1996), supernova remnants (e.g. Dennefeld & Péquignot 1983; Dennefeld 1986; Hudgins et al. 1990; Rudy et al. 1994), and circumstellar nebulae (e.g. Stahl & Wolf 1986; Johnson et al. 1992). Quite generally, accurate calculations of atomic data for all nickel ions, particularly the low ionization stages are important in astronomy.

The IRON Project is an international collaboration devoted to the computation of accurate atomic data for iron group elements (Hummer et al. 1993). A complete list of papers including those in press can be found at `http://www.am.qub.uk/projects/iron/papers/`. The present paper reports extensive electron impact excitation data, line emissivities, and emissivity line ratios for Ni III. This is only the second time such calculations for this ion are performed. The first collisional calculation for Ni III was carried out by Watts & Burke (1998; WB heretherein), yet their computations were carried out in *LS* coupling only which makes the results of little practical use.

2. Target expansion

In the close coupling (CC) approximation the total wave function of the electron-ion system is represented as

$$\Psi(E; SL\pi) = A \sum_i \chi_i \theta_i + \sum_j c_j \Phi_j, \qquad (1)$$

where χ_i is the target ion wave function in a specific state $S_i\ L_i$, θ_i is the wave function for the free electron, and Φ_j are short range correlation functions for the bound (e+ion) system. Accurate CC calculations of atomic processes require a good representation of the target ion. For complex ions an accurate representation must include a large number of correlation configurations. However, in order for the computations to be computationally tractable, the configuration expansion must be carefully and economically chosen.

The target expansion employed in the present calculation is based on the target used by Bautista (1999) in the calculation of radiative data for Ni II. The atomic

Send offprint requests to: M. A. Bautista
e-mail: `bautista@lhea1.gsfc.nasa.gov`

* Tables 1 to 5 are also available at the CDS via anonymous ftp to `cdsarc.u-strasbg.fr` (130.79.128.5) or via `http://cdsweb.u-strasbg.fr/cgi-bin/qcat?J/A+A/365/268`

Table 1. Energy levels in Rydbergs for the Ni III ion relative to the $3d^8(^3F)$ ground state. The present calculated energies are compared with experimentally determined energies and those calculated by Watts & Burke (WB). The spectroscopic and correlation configurations for Ni III, and the values of the scaling parameters λ_{nl} for each orbital in the Thomas-Fermi-Dirac potential used in Superstructure are also given

	Level		Experimental	Present	WB		Level		Experimental	Present	WB
1	$3d^8$	^{3}F	0.00000	0.00000	0.0000	36	$3d^7(^4P)4p$	^{3}D°	1.20764	1.17313	1.1591
2	$3d^8$	^{1}D	0.11881	0.15138	0.1530	37	$3d^7(^2G)4p$	^{3}G°	1.21295	1.19463	1.1521
3	$3d^8$	^{3}P	0.14431	0.16910	0.1724	38	$3d^7(^2G)4p$	^{1}H°	1.21402	1.15889	1.1499
4	$3d^8$	^{1}G	0.20152	0.23027	0.2333	39	$3d^7(^2G)4p$	^{1}F°	1.22136	1.17331	1.1673
5	$3d^8$	^{1}S	0.46965	0.56320	0.5693	40	$3d^7(^4P)4p$	^{3}P°	1.22660	1.17770	1.1857
6	$3d^7(^4F)4s$	^{5}F	0.49063	0.43192	0.4345	41	$3d^7(^2P)4p$	^{3}D°	1.23933	1.21491	1.2093
7	$3d^7(^4F)4s$	^{3}F	0.55838	0.50696	0.5112	42	$3d^7(^2P)4p$	^{1}D°	1.24510	1.21149	1.2057
8	$3d^7(^4P)4s$	^{5}P	0.64093	0.61541	0.6196	43	$3d^7(^2H)4p$	^{3}I°	1.24696	1.19688	1.1866
9	$3d^7(^2G)4s$	^{3}G	0.67974	0.64029	0.6533	44	$3d^7(^2H)4p$	^{3}G°	1.24677	1.15834	1.1864
10	$3d^7(^4P)4s$	^{3}P	0.70540	0.69345	0.6985	45	$3d^7(^2G)4p$	^{1}S°	1.24983	1.21895	1.2131
11	$3d^7(^2G)4s$	^{1}G	0.71312	0.67760	0.6911	46	$3d^7(^2G)4p$	^{3}D°	1.25616	1.22231	1.2161
12	$3d^7(^2P)4s$	^{3}P	0.71548	0.70220	0.7165	47	$3d^7(^4P)4p$	^{1}I°	1.26338	1.20874	1.1989
13	$3d^7(^2H)4s$	^{3}H	0.73970	0.70229	0.7153	48	$3d^7(^2P)4p$	^{3}F°	1.27101	1.23541	1.2299
14	$3d^7(a\ ^2D)4s$	^{3}D	0.64256	0.72358	0.7390	49	$3d^7(^2H)4p$	^{3}S°	1.27478	1.25482	1.2557
15	$3d^7(^2P)4s$	^{1}P	0.76191	0.73984	0.7550	50	$3d^7(^2H)4p$	^{1}P°	1.27960	1.27078	1.2486
16	$3d^7(^2H)4s$	^{1}H	0.77312	0.73884	0.7526	51	$3d^7(^2G)4p$	^{1}D°	1.28890	1.26425	1.2598
17	$3d^7(a^2D)4s$	^{1}D	0.78052	0.76212	0.7777	52	$3d^7(^2G)4p$	^{3}H°	1.28986	1.24017	1.2364
18	$3d^7(^2F)4s$	^{3}F	0.88456	0.88604	0.9030	53	$3d^7(a^2D)4p$	^{1}F°	1.30193	1.26710	1.2662
19	$3d^7(^2F)4s$	^{1}F	0.92002	0.92621	0.9430	54	$3d^7(a^2D)4p$	^{3}P°	1.30394	1.27065	1.2702
20	$3d^7(^4F)4p$	^{5}F°	1.00141	0.93138	0.9116	55	$3d^7(^2H)4p$	^{1}G°	1.30456	1.26040	1.2616
21	$3d^7(^4F)4p$	^{5}D°	1.01975	0.94546	0.9272	56	$3d^7(a^2D)4p$	^{1}P°	1.32094	1.29308	1.2952
22	$3d^7(^4F)4p$	^{5}G°	1.02468	0.94404	0.9341	57	$3d^7(^2H)4p$	^{1}H°	1.32436	1.28011	1.2797
23	$3d^7(^4F)4p$	^{3}G°	1.05115	0.98332	0.9650	58	$3d^6\ 4s^2$	^{5}D	1.39116	1.67319	—
24	$3d^7(^4F)4p$	^{3}F°	1.05715	0.99140	0.9758	59	$3d^7(^2F)4p$	^{1}D°	1.40405	1.39724	1.3949
25	$3d^7(^4F)4p$	^{3}D°	1.07862	1.01563	1.0032	60	$3d^7(^2F)4p$	^{3}G°	1.41372	1.40245	1.4011
26	$3d^7(^4F)4s$	^{3}D	1.09859	1.13533	0.9272	61	$3d^7(^2F)4p$	^{3}F°	1.41870	1.40517	1.4049
27	$3d^7(^4P)4p$	^{5}S°	1.10526	1.06400	1.0416	62	$3d^7(^2F)4p$	^{3}D°	1.42190	1.40991	1.4100
28	$3d^7(^4P)4s$	^{1}D	1.13400	1.17534	1.2001	63	$3d^7(^2F)4p$	^{1}G°	1.42505	1.41456	1.4113
29	$3d^7(^4P)4p$	^{5}D°	1.17636	1.13882	1.1239	64	$3d^7(^2F)4p$	^{1}F°	1.46496	1.45926	1.4607
30	$3d^7(^4P)4p$	^{3}S°	1.18346	1.15889	1.1447	65	$3d^7(b^2D)4p$	^{3}P°	1.59975	1.62133	1.6258
31	$3d^7(^2G)4p$	^{3}H°	1.19329	1.14180	1.1322	66	$3d^7(b^2D)4p$	^{3}F°	1.61895	1.64261	1.6492
32	$3d^7(^2G)4p$	^{3}F°	1.20136	1.15002	1.1443	67	$3d^7(b^2D)4p$	^{1}P°	1.64219	1.67025	1.6795
33	$3d^7(^4P)4p$	^{5}P°	1.20340	1.16800	1.1562	68	$3d^7(b^2D)4p$	^{1}F°	1.64633	1.67426	1.6796
34	$3d^7(^2G)4p$	^{1}G°	1.20589	1.15878	1.1430	69	$3d^7(b^2D)4p$	^{3}D°	1.66984	1.69755	1.7097
35	$3d^7(^2P)4p$	^{3}P°	1.20688	1.17770	1.1694	70	$3d^7(b^2D)4p$	^{1}D°	1.79860	1.69812	1.7088

Ni III configurations.
Spectroscopic: $3p^6\ 3d^8$, $3p^6\ 3d^7\ 4s$, $3p^6\ 3d^7\ 4p$, $3p^6\ 3d^6\ 4s^2$.
Correlation: $3p^6\ 3d^6\ 4p^2$, $3p^6\ 3d^7\ 4d$, $3p^6\ 3d^6\ 4s\ 4p$, $3p^5\ 3d^9$, $3p^5\ 3d^8\ 4s$, $3p^5\ 3d^8\ 4p$, $3p^5\ 3d^8\ 4d$.
λ_{nl}: 1.43121(1s), 0.93950(2s), 1.28641(2p), 1.15714(3s), 1.02417(3p), 1.01626(3d), 0.97488(4s), 0.96711(4p), 1.26086(4d).

structure code SUPERSTRUCTURE (Eissner et al. 1974) was used to compute eigenfunctions for the target states dominated by the configurations $3d^8$, $3d^7\,4s$, $3d^7\,4p$, and $3d^6\,4s^2$. Table 1 presents the list of spectroscopic and correlation configurations in the target and the *LS* states included in the CC expansion. The table also shows a comparison between the calculated target term energies, the observed energies averaged over the fine structure taken from Sugar & Corliss (1985), and the calculated energies by WB. The agreement between the present energies and experiment is good; in all but the lowest five terms the discrepancy is less than 9%. The overall error is approximately 5%. The target energies of WB are very similar to the present ones, but the agreement with experiment is slightly worse. Some discrepancies appear between the calculated relative ordering of the multiplets 53 through 70 and experiment. Laboratory spectra show that these states are mixed with $3d^7$ 4d and $3d^7$ 5s states. Thus, it is likely that the representation of the highly excited $3d^7$ 4p states is somewhat inaccurate due to missing correlations. Yet, to improve the representation of the high $3d^7$ 4p states it would be necessary to include many more configurations in the target which would make the scattering calculation too large for current computational resources. Nevertheless, it has been found that such states must be included in the CC expansion because they

Table 2. Comparison between present and NIST radiative transition rates (A-values) for allowed transitions. A-values are given in units of 10^8 s^{-1}

Transition	NIST	Present
$3d^7(^4F)4s\ ^5F_5 - 3d^7(^4F)4p\ ^5G^\circ_4$	0.038	0.0269
$3d^7(^4F)4s\ ^5F_5 - 3d^7(^4F)4p\ ^5G^\circ_6$	7.9	8.28
$3d^7(^4F)4s\ ^5F_4 - 3d^7(^4F)4p\ ^5G^\circ_5$	6.3	7.76
$3d^7(^4F)4s\ ^5F_2 - 3d^7(^4F)4p\ ^5G^\circ_3$	6.0	7.25
$3d^7(^4F)4s\ ^5F_1 - 3d^7(^4F)4p\ ^5G^\circ_2$	5.9	7.08
$3d^7(^4F)4s\ ^5F_1 - 3d^7(^4F)4p\ ^5D^\circ_0$	6.7	7.63
$3d^7(^4F)4s\ ^3F_4 - 3d^7(^4F)4p\ ^3D^\circ_3$	5.7	5.75
$3d^7(^4F)4s\ ^3F_3 - 3d^7(^4F)4p\ ^3D^\circ_2$	5.5	5.75
$3d^7(^4F)4s\ ^3F_2 - 3d^7(^4F)4p\ ^3D^\circ_1$	6.5	7.28
$3d^7(^4F)4s\ ^5F_5 - 3d^7(^4F)4p\ ^5F^\circ_5$	6.2	7.38
$3d^7(^4F)4s\ ^5F_1 - 3d^7(^4F)4p\ ^5F^\circ_1$	3.8	4.05
$3d^7(^4F)4s\ ^5F_2 - 3d^7(^4F)4p\ ^5F^\circ_2$	2.5	2.84
$3d^7(^4F)4s\ ^5F_3 - 3d^7(^4F)4p\ ^5F^\circ_3$	2.5	2.93
$3d^7(^4F)4s\ ^5F_4 - 3d^7(^4F)4p\ ^5F^\circ_4$	2.7	3.46
$3d^7(^4F)4s\ ^3F_4 - 3d^7(^4F)4p\ ^3F^\circ_4$	5.6	5.30
$3d^7(^4F)4s\ ^3F_3 - 3d^7(^4F)4p\ ^3F^\circ_3$	4.6	4.27
$3d^7(^4F)4s\ ^3F_2 - 3d^7(^4F)4p\ ^3F^\circ_2$	5.0	5.03
$3d^7(^4F)4s\ ^3F_3 - 3d^7(^4F)4p\ ^3G^\circ_4$	5.3	5.04
$3d^7(^4F)4s\ ^3F_4 - 3d^7(^4F)4p\ ^3G^\circ_5$	5.4	6.09

significantly affect the collision strengths for some transitions (see Sect. 3).

Other indicators of the accuracy of the present target representation are the good agreement between the length and the velocity oscillator strengths, typically within 10–20%, and between present radiative transition probabilities for allowed transitions and recommended values by NIST (Fuhr et al. 1988). Table 2 shows the comparison between the present A-values and all values available from NIST. Notice the NIST data has an accuracy rating D throughout (i.e. estimated uncertainty of ∼40%)

3. Calculations

The computations were carried out with the RMATRX package of codes (Berrington et al. 1995). The $(N+1)-$electron wavefunctions set on the right hand side of the CC expansion in Eq. (1) includes all possible configurations of the form $3p^6\ 3d^i4s^j4p^k4d^l$, with $7 \le i \le 9$, $0 \le j \le 2$, $0 \le k \le 3$, and $0 \le l \le 2$.

The calculation of the scattering matrices was carried out in LS coupling. The fine structure collision strengths were obtained by algebraic transformation of the scattering matrices to pair coupling scheme. This is a reasonably accurate procedure for $3d^8$ and $3d^7\,4s$ configurations of Ni III for which relativistic effects seem small, as suggested by the fact that the observed fine structure energy splitting is much smaller than the energy difference between consecutive energy terms. In order to further ensure that fine structure corrections to collision strengths are small, a 9-level Breit-Pauli calculation was carried out for the $3p^63d^8$ ground configuration only. It was found that the collision strengths from the Breit-Pauli and the calculations using just algebraic transformations differed by less than ∼1%. In the case of the levels from the $3d^7\,4p$ configuration, however, it is likely that relativistic effects will be significant given the level of mixing observed for the energy levels. On the other hand, a relativistic calculation of all the $3d^7\,4p$ level would be computationally prohibitive. Moreover, the accuracy of the collision strengths for these levels is of only minor importance since they produce no observable emission lines under collisional excitation. Yet, including the $3d^7\,4p$ levels in the population equilibrium model of Ni III may be important for fluorescent excitation and recombination conditions.

Partial wave contributions are included from 78 $SL\,\pi$ total symmetries with angular momentum $L = 0 - 12$, total multiplicities $(2S+1) = 2$, 4, and 6, and parities even and odd. Additional "top-up" was calculated for dipole transitions using the Burgess sum rules.

The collision strengths were calculated at nearly 21 000 energy points from 0 to 8 Ry, with most of the points in the near threshold regions as to properly resolve resonances. These number of energy points provides sufficiently good resolution for accurate calculations of effective collision strengths.

Two sets of calculations were carried out for different CC expansions. The first calculation included the lowest 52 LS terms from Table 1. A second calculation including all 70 states was necessary because, as pointed out by Burke (2000, private communication), there is significant collisional coupling between some $3d^7$ 4s states and highly excited $3d^7$ 4p states. Table 3 compares the LS effective collision strengths from the ground state into excited multiplets from both calculations. The $3d^7$ 4p states 53 through 70 are found to change the collision strength by a factor of ∼3 for two transitions from the ground to the highest $3d^7$ 4s states. Apart from these, there are three transitions that change by ∼30%, while the discrepancy for all other transitions is less than 20%. Based on these comparison it is decided to employ the 70CC expansion for the rest of this work.

4. Results: Collision strengths

Figures 1a-d show the collision strengths summed over fine structure for the transitions $3d^8(^3F-^1D)$, $(^3F-^3P)$, $3d^8(^3F-^1G)$, and $3d^8(^3F-^1S)$. These collision strengths correspond to those presented in Figs. 1–4 of the WB paper. Good qualitative agreement between both calculations is observed. There is, however, much better resolution of the resonances in the present calculation.

Table 4 compares the effective collision strengths for forbidden transition from the ground state from the present calculation summed over fine structure with the results of WB. For most transitions the effective collision strengths agree within 10–20%. Most of the differences between the two sets of effective collision strengths seem to arise from the improve resolution of the resonances in

Table 3. Comparison of effective collision strengths in LS coupling at $T = 10^4$ K for excitations from the ground term to the first 51 excited terms

	Final state	Υ(52CC)	Υ(70CC)	$\frac{\Upsilon(70CC)}{\Upsilon(52CC)}$
2	$3d^8\ ^1D$	1.482	1.804	1.217
3	$3d^8\ 4s\ ^3P$	5.018	5.064	1.009
4	$3d^8\ 4s\ ^1G$	3.126	3.115	0.997
5	$3d^8\ 4s\ ^1S$	0.108	0.149	1.381
6	$3d^7\ 4s\ ^5P$	6.222	6.109	0.982
7	$3d^7\ 4s\ ^3F$	8.026	9.237	1.151
8	$3d^7\ 4s\ ^5P$	1.434	1.571	1.096
9	$3d^7\ 4s\ ^3G$	6.246	7.212	1.155
10	$3d^7\ 4s\ ^3P$	1.387	1.612	1.163
11	$3d^7\ 4s\ ^1G$	0.822	0.946	1.151
12	$3d^7\ 4s\ ^3P$	1.560	1.748	1.121
13	$3d^7\ 4s\ ^3H$	6.193	6.611	1.068
14	$3d^7\ 4s\ ^3D$	2.787	2.752	0.987
15	$3d^7\ 4s\ ^1P$	0.458	0.457	0.998
16	$3d^7\ 4s\ ^1H$	1.030	0.789	0.766
17	$3d^7\ 4s\ ^1D$	0.608	0.554	0.911
18	$3d^7\ 4s\ ^3F$	1.221	0.874	0.715
19	$3d^7\ 4s\ ^1F$	0.272	0.079	0.292
20	$3d^7\ 4p\ ^5F^\circ$	1.968	2.016	1.024
21	$3d^7\ 4p\ ^5D^\circ$	1.032	1.111	1.076
22	$3d^7\ 4p\ ^5G^\circ$	1.777	1.871	1.053
23	$3d^7\ 4p\ ^3G^\circ$	2.058	2.055	0.998
24	$3d^7\ 4p\ ^3F^\circ$	6.761	6.880	1.018
25	$3d^7\ 4p\ ^3D^\circ$	3.932	4.034	1.026
26	$3d^7\ 4s\ ^3D$	0.381	0.248	0.650
27	$3d^7\ 4p\ ^5S^\circ$	0.241	0.245	1.019
28	$3d^7\ 4s\ ^1D$	0.094	0.027	0.292
29	$3d^7\ 4p\ ^5D^\circ$	0.466	0.457	0.979
30	$3d^7\ 4p\ ^3S^\circ$	0.108	0.100	0.924
31	$3d^7\ 4p\ ^3H^\circ$	0.756	0.777	1.028
32	$3d^7\ 4p\ ^3F^\circ$	4.698	4.784	1.018
33	$3d^7\ 4p\ ^5P^\circ$	0.273	0.259	0.949
34	$3d^7\ 4p\ ^1G^\circ$	0.258	0.268	1.037
35	$3d^7\ 4p\ ^3P^\circ$	0.270	0.243	0.902
36	$3d^7\ 4p\ ^3D^\circ$	0.800	0.774	0.969
37	$3d^7\ 4p\ ^3G^\circ$	1.325	1.317	0.993
38	$3d^7\ 4p\ ^1H^\circ$	0.193	0.183	0.947
39	$3d^7\ 4p\ ^1F^\circ$	0.146	0.139	0.955
40	$3d^7\ 4p\ ^3P^\circ$	0.222	0.208	0.937
41	$3d^7\ 4p\ ^3D^\circ$	0.527	0.736	1.398
42	$3d^7\ 4p\ ^1D^\circ$	0.072	0.065	0.910
43	$3d^7\ 4p\ ^3I^\circ$	0.693	0.650	0.938
44	$3d^7\ 4p\ ^3G^\circ$	5.617	5.648	1.005
45	$3d^7\ 4p\ ^1S^\circ$	0.010	0.009	0.889
46	$3d^7\ 4p\ ^3D^\circ$	3.308	3.332	1.007
47	$3d^7\ 4p\ ^1I^\circ$	0.214	0.214	0.997
48	$3d^7\ 4p\ ^3F^\circ$	0.863	0.887	1.028
49	$3d^7\ 4p\ ^3S^\circ$	0.038	0.031	0.823
50	$3d^7\ 4p\ ^1P^\circ$	0.022	0.019	0.860
51	$3d^7\ 4p\ ^1D^\circ$	0.062	0.061	0.986
52	$3d^7\ 4p\ ^3H^\circ$	0.369	0.363	0.985

the present calculation. Notice that the present calculation uses about twenty times as many points as in WB.

Effective collision strengths for all transitions considered here have been calculated for several temperatures between 5 000 and 100 000 K. These data is expected

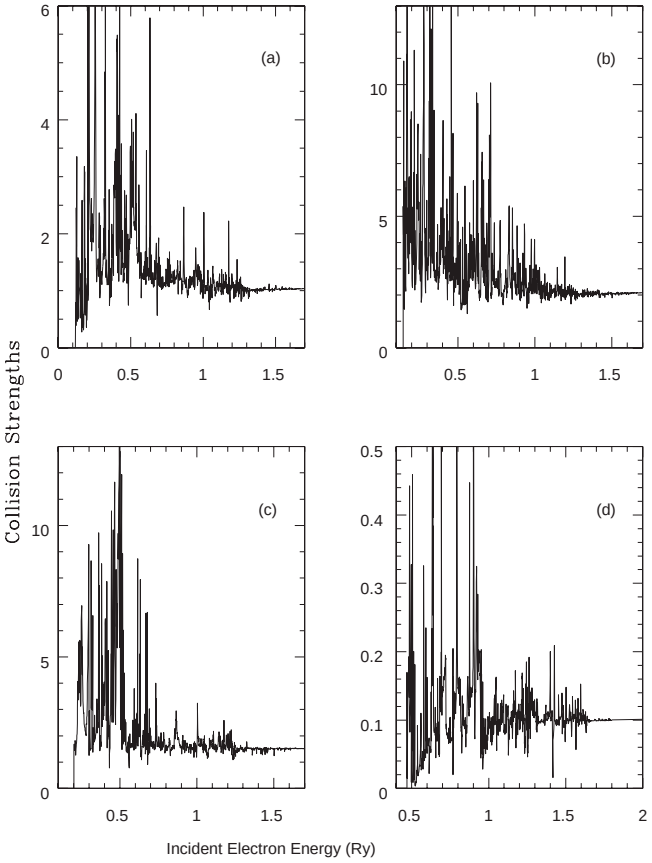

Fig. 1. Collision strengths for Ni III, in LS coupling, for transitions: **a)** $3d^8(^3F\text{-}\ ^1D)$; **b)** $3d^8(^3F{-}^3P)$; **c)** $3d^8(^3F{-}^1G)$; **d)** $3d^8(^3F{-}^1S)$

Table 4. Comparison of effective collision strengths in LS coupling from the present calculation and those of WB. The level indices refer to the entries in Table 1

Trans.	5000 K		10 000 K		20 000 K	
	Present	WB	Present	BW	Present	WB
1-2	1.25	1.37	1.48	1.48	1.70	1.56
1-3	5.17	4.03	5.02	4.19	4.69	4.19
1-4	2.80	2.24	3.13	2.52	3.30	2.71
1-5	0.126	0.137	0.110	0.118	0.109	0.112
1-6	6.29	5.49	6.14	5.83	5.60	5.52
1-7	8.09	7.75	7.99	7.86	7.65	7.54
1-8	1.47	1.43	1.38	1.32	1.28	1.22
1-9	7.05	5.25	6.21	5.08	5.31	4.59
1-10	1.34	1.68	1.39	1.54	1.34	1.40
1-11	0.830	1.03	0.814	0.972	0.774	0.876
1-12	1.67	1.23	1.54	1.27	1.32	1.17
1-13	7.03	6.39	6.24	6.00	5.37	5.13
1-14	2.82	2.28	2.86	2.45	2.57	2.31
1-15	0.589	0.504	0.442	0.413	0.329	0.320
1-16	0.967	1.03	1.03	1.09	0.978	1.03
1-17	0.682	0.677	0.615	0.624	0.520	0.531
1-18	1.01	0.843	1.21	1.13	1.27	1.25
1-19	0.262	0.292	0.266	0.302	0.240	0.270
1-26	0.337	0.374	0.389	0.416	0.375	0.392
1-28	0.105	0.096	0.096	0.091	0.079	0.078

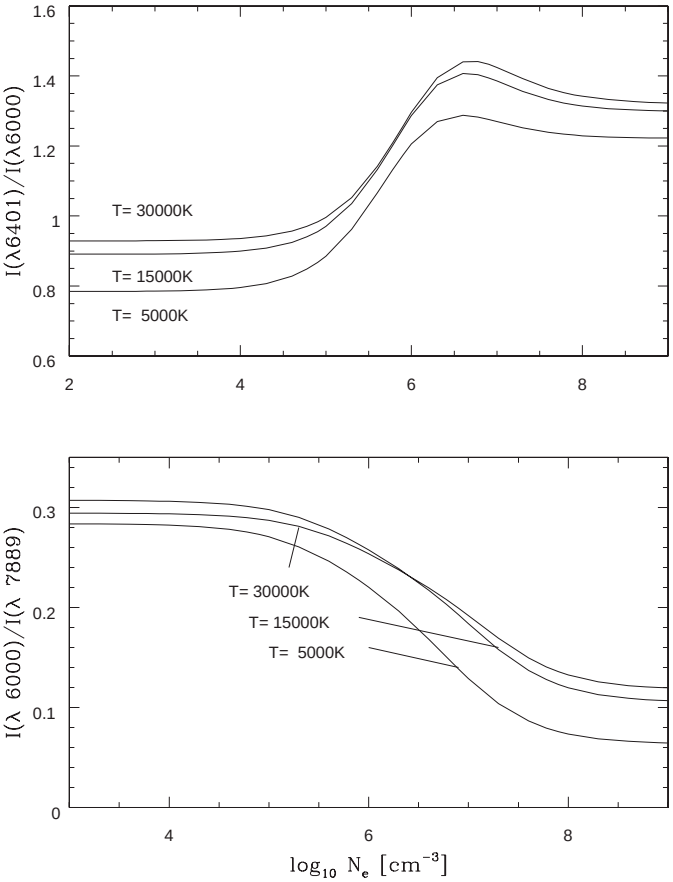

Fig. 2. Line ratio diagnostics of electron density from optical lines of Ni III

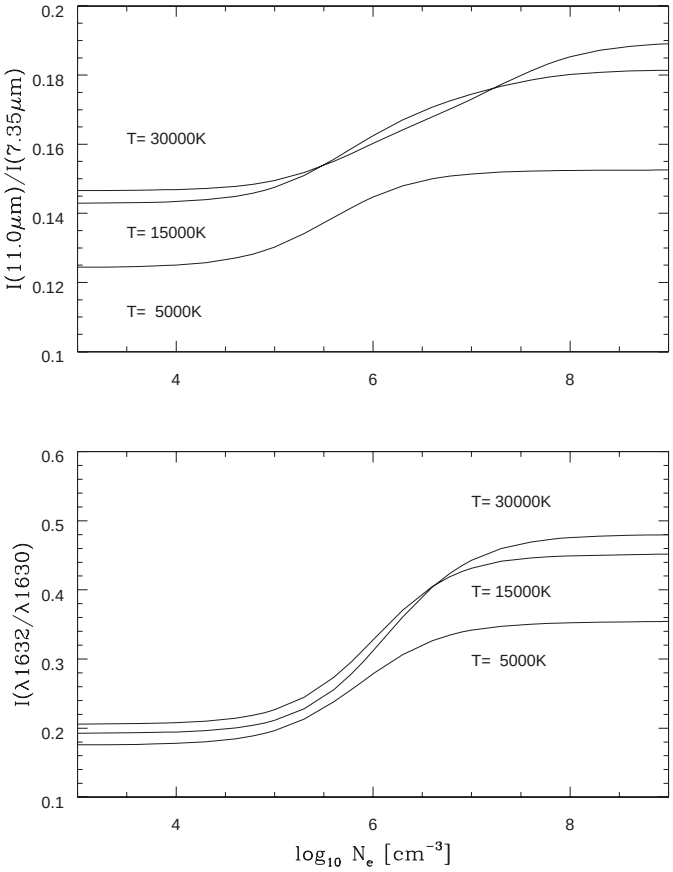

Fig. 3. Line ratio diagnostics of electron density from IR and UV lines of Ni III

to be accurate to 10–20% for transitions between levels of the $3d^8$ and $3d^7$ 4s configurations, but less accurate for transition that involve levels of the $3d^7$ 4p configuration.

5. The Ni III emission spectra

The collision strengths computed here were used to build a collisional-radiative model for Ni III. The energy levels for this model were taken from Sugar & Corliss (1985). We use theoretical transition probabilities for forbidden transitions from Garstang (1958) and A-values calculated with SUPERSTRUCTURE.

The emission spectra under collisional excitation were calculated for wide ranges of density and temperature and the strongest lines were identified. These lines are ($3d^8$ $^3F_4 - {}^3F_3$) at 7.347 μm and ($3d^8$ $^3F_3 - {}^3F_2$) at 11 000 μm in the IR; ($3d^8$ $^3F_{3,2} - {}^1D_2$) at 7889.9 and 8499.6 Å, ($3d^8$ $^3F_{4,3} - {}^3P_2$) at 6000.2 and 6533.8 Å, ($3d^8$ $^3F_3 - {}^3P_1$) at 6401.5 Å, and ($3d^8$ $^3F_{4,3} - {}^1G_4$) at 4326.2 and 4596.9 Å in the optical; and ($3d^8$ $^3F_4 - 3d^7 4s$ $^3F_4$) at 1629.9 Å and ($3d^8$ $^3F_3 - 3d^7 4s$ $^3F_3$) at 1632.3 Å in the UV.

Density diagnostics can be obtained from IR, optical, or UV lines as illustrated in Figs. 2 and 3. It can be seen from Fig. 2 that the $I(\lambda6401)/I(\lambda6000)$ and $I(\lambda6000)/I(\lambda7889)$ optical line ratios are sensitive to variations of the electron density between 10^4 and 10^7 cm^3. Similarly, the IR and UV line ratios $I(11.0\ \mu\text{m})/I(7.35\ \mu\text{m})$ and $I(\lambda1632)/I(\lambda1630)$ shown in Fig. 3 can be used as density diagnostics for electron densities between $\sim 10^5$ and $\sim 3\ 10^6$ cm^{-3}.

On the other hand, emissivity line ratios of either the 4326.2 or 4596.9 Å lines to any of the other optical lines are useful in diagnosing the temperature of the plasma. Two of these line ratios are shown in Figs. 4 and 5.

Table 3 presents line emissivities for the most important optical and IR lines for several temperature and electron density values. Here the emissivity per Ni III ion of the λ6000 lines is given in erg/s, and the intensity of all other lines is given with respect to this one.

6. Conclusion

Collision strengths and effective collision strengths are reported for 162 levels from configurations $3d^8$, $3d^7 4s$, $4d^7 4p$, and $3d^6 4s^2$ of Ni III. The calculations were carried out using the R-matrix method. The present results are in good agreement with the previous calculations for this ion by WB.

A collisional-radiative model for Ni III is constructed with the present data. Then, the model is used to identify the strongest IR, optical, and UV emission lines under collisional excitation conditions. The line emissivities for these features and several density and temperature line ratio diagnostics are given.

Table 5. Line emissivities for the strongest optical and IR Ni III lines. The emissivity per Ni^{2+} ion of the λ6000 line is given in erg/s. The emissivity of other lines is relative to that of λ6000

T	N_e	$j(\lambda6000)$	$I(7.35\ \mu m)$	$I(11\ \mu m)$	$I(\lambda7889)$	$I(\lambda8499)$	$I(\lambda6533)$	$I(\lambda6401)$	$I(\lambda4326)$	$I(\lambda4596)$
5.0E+3	1.E+02	1.03E-20	8.46E+1	1.05E+1	3.53E+0	1.43E+0	2.19E+0	7.84E-1	6.18E-1	2.99E-1
	1.E+04	1.02E-18	8.35E+1	1.04E+1	3.54E+0	1.44E+0	2.19E+0	7.96E-1	6.22E-1	3.01E-1
	1.E+06	8.19E-17	3.96E+1	5.73E+0	4.54E+0	1.84E+0	2.19E+0	1.21E+0	8.51E-1	4.12E-1
	1.E+08	3.98E-16	1.26E+1	1.92E+0	1.36E+1	5.52E+0	2.19E+0	1.23E+0	2.49E+0	1.21E+0
	1.E+10	4.14E-16	1.22E+1	1.86E+0	1.57E+1	6.37E+0	2.19E+0	1.22E+0	2.73E+0	1.32E+0
1.0E+4	1.E+02	7.67E-20	1.12E+1	1.56E+0	3.23E+0	1.31E+0	2.19E+0	8.61E-1	1.82E+0	8.82E-1
	1.E+04	7.64E-18	1.11E+1	1.55E+0	3.25E+0	1.32E+0	2.19E+0	8.71E-1	1.83E+0	8.86E-1
	1.E+06	6.07E-16	5.63E+0	9.03E-1	3.93E+0	1.60E+0	2.19E+0	1.27E+0	2.35E+0	1.14E+0
	1.E+08	3.55E-15	1.42E+0	2.47E-1	9.38E+0	3.81E+0	2.19E+0	1.29E+0	6.24E+0	3.02E+0
	1.E+10	3.73E-15	1.35E+0	2.34E-1	1.08E+1	4.36E+0	2.19E+0	1.28E+0	6.90E+0	3.34E+0
1.5E+4	1.E+02	1.34E-19	6.14E+0	8.77E-1	3.26E+0	1.32E+0	2.19E+0	8.91E-1	2.69E+0	1.30E+0
	1.E+04	1.34E-17	6.08E+0	8.72E-1	3.27E+0	1.33E+0	2.19E+0	9.00E-1	2.70E+0	1.31E+0
	1.E+06	1.06E-15	3.22E+0	5.23E-1	3.88E+0	1.58E+0	2.19E+0	1.29E+0	3.37E+0	1.63E+0
	1.E+08	6.76E-15	6.98E-1	1.26E-1	8.35E+0	3.39E+0	2.19E+0	1.31E+0	8.46E+0	4.09E+0
	1.E+10	7.11E-15	6.46E-1	1.17E-1	9.48E+0	3.85E+0	2.19E+0	1.30E+0	9.40E+0	4.55E+0
2.0E+4	1.E+02	1.68E-19	4.68E+0	6.76E-1	3.31E+0	1.34E+0	2.19E+0	9.09E-1	3.30E+0	1.60E+0
	1.E+04	1.67E-17	4.64E+0	6.72E-1	3.32E+0	1.35E+0	2.19E+0	9.17E-1	3.32E+0	1.60E+0
	1.E+06	1.33E-15	2.54E+0	4.11E-1	3.90E+0	1.58E+0	2.19E+0	1.30E+0	4.07E+0	1.97E+0
	1.E+08	8.86E-15	4.94E-1	9.05E-2	7.90E+0	3.21E+0	2.19E+0	1.33E+0	9.85E+0	4.77E+0
	1.E+10	9.25E-15	4.48E-1	8.32E-2	8.91E+0	3.62E+0	2.19E+0	1.31E+0	1.10E+1	5.31E+0
3.0E+4	1.E+02	1.95E-19	3.66E+0	5.36E-1	3.40E+0	1.38E+0	2.19E+0	9.29E-1	4.05E+0	1.96E+0
	1.E+04	1.94E-17	3.63E+0	5.33E-1	3.41E+0	1.38E+0	2.19E+0	9.36E-1	4.07E+0	1.97E+0
	1.E+06	1.55E-15	2.09E+0	3.34E-1	3.94E+0	1.60E+0	2.19E+0	1.30E+0	4.89E+0	2.36E+0
	1.E+08	1.08E-14	3.62E-1	6.70E-2	7.55E+0	3.06E+0	2.19E+0	1.34E+0	1.15E+1	5.54E+0
	1.E+10	1.07E-14	3.14E-1	5.96E-2	8.40E+0	3.41E+0	2.19E+0	1.32E+0	1.28E+1	6.20E+0
4.0E+4	1.E+02	2.01E-19	3.27E+0	4.86E-1	3.46E+0	1.41E+0	2.19E+0	9.40E-1	4.44E+0	2.15E+0
	1.E+04	2.01E-17	3.25E+0	4.83E-1	3.47E+0	1.41E+0	2.19E+0	9.47E-1	4.45E+0	2.15E+0
	1.E+06	1.60E-15	1.94E+0	3.09E-1	3.99E+0	1.62E+0	2.19E+0	1.29E+0	5.28E+0	2.56E+0
	1.E+08	1.13E-14	3.22E-1	5.99E-2	7.46E+0	3.03E+0	2.19E+0	1.35E+0	1.23E+1	5.97E+0
	1.E+10	1.06E-14	2.68E-1	5.14E-2	8.20E+0	3.33E+0	2.19E+0	1.32E+0	1.38E+1	6.67E+0
5.0E+4	1.E+02	2.01E-19	3.07E+0	4.61E-1	3.50E+0	1.42E+0	2.19E+0	9.43E-1	4.61E+0	2.23E+0
	1.E+04	2.00E-17	3.05E+0	4.58E-1	3.51E+0	1.42E+0	2.19E+0	9.50E-1	4.63E+0	2.24E+0
	1.E+06	1.60E-15	1.88E+0	2.98E-1	4.01E+0	1.63E+0	2.19E+0	1.29E+0	5.45E+0	2.64E+0
	1.E+08	1.14E-14	3.09E-1	5.76E-2	7.47E+0	3.03E+0	2.19E+0	1.36E+0	1.28E+1	6.21E+0
	1.E+10	1.01E-14	2.49E-1	4.79E-2	8.13E+0	3.30E+0	2.19E+0	1.32E+0	1.44E+1	6.95E+0
6.0E+4	1.E+02	1.98E-19	2.96E+0	4.47E-1	3.53E+0	1.43E+0	2.19E+0	9.43E-1	4.71E+0	2.28E+0
	1.E+04	1.97E-17	2.94E+0	4.45E-1	3.54E+0	1.44E+0	2.19E+0	9.49E-1	4.72E+0	2.28E+0
	1.E+06	1.57E-15	1.85E+0	2.94E-1	4.04E+0	1.64E+0	2.19E+0	1.28E+0	5.54E+0	2.68E+0
	1.E+08	1.12E-14	3.07E-1	5.74E-2	7.53E+0	3.06E+0	2.19E+0	1.36E+0	1.32E+1	6.38E+0
	1.E+10	9.56E-15	2.41E-1	4.64E-2	8.11E+0	3.29E+0	2.19E+0	1.32E+0	1.47E+1	7.13E+0

Several of the strongest lines in the optical have been observed in H II region like the Orion nebula. For example, the λ7889.9 line was measured by Osterbrock et al. (1992) and the $\lambda\lambda$ 6000.2, 4101.5, and 6533.8 features were reported by Esteban et al. (1998). From the observed λ7889.9 line and empirically estimates of [Ni III] collision strengths, Osterbrock et al. derived a value for the Ni^{2+} abundance. The value of Osterbrock et al. for the $^3F_4 - {}^1D_2$ transition that leads to the λ7889.9 line is only off by 30%. On the other hand, other collision strengths from Osterbrock et al. needed to analyze the $\lambda\lambda$ 6000.2, 4101.5, and 6533.8 lines are underestimated by factors of three to five, and for other transitions the errors are as high as a factor of nine.

Acknowledgements. I like to thank Mrs. V. Burke for pointing out to me the importance of including the highest $3d^7$ 4p states in the CC expansion. The computations were carried out on the CRAY J94 at the NASA Center for Computational Sciences and the CRAY T3E at the High Performance Computing and Communications Program at NASA/GSFC.

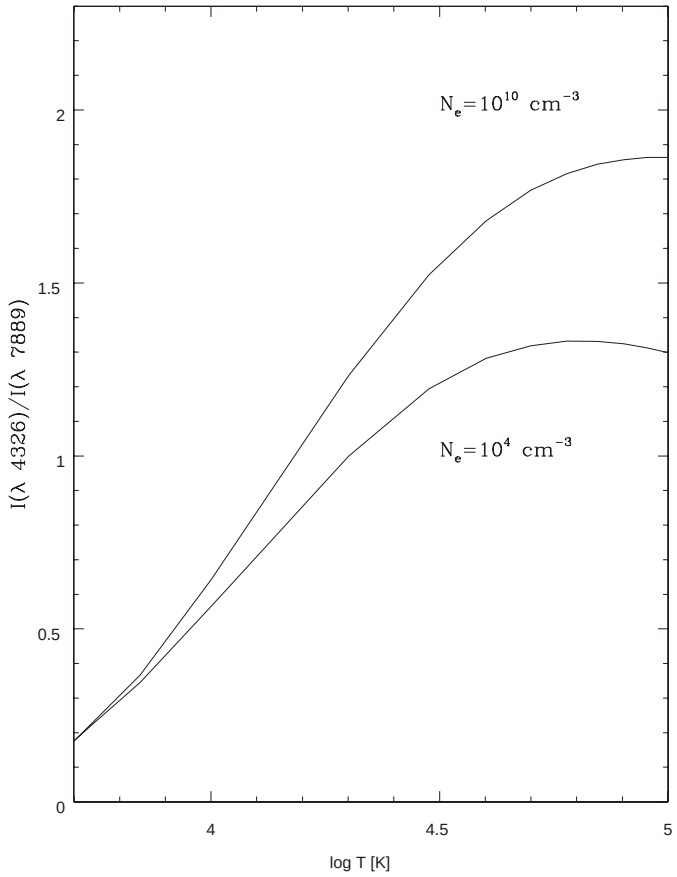

Fig. 4. λ4326 to λ7889 ratio as temperature diagnostic for two different values of the electron density

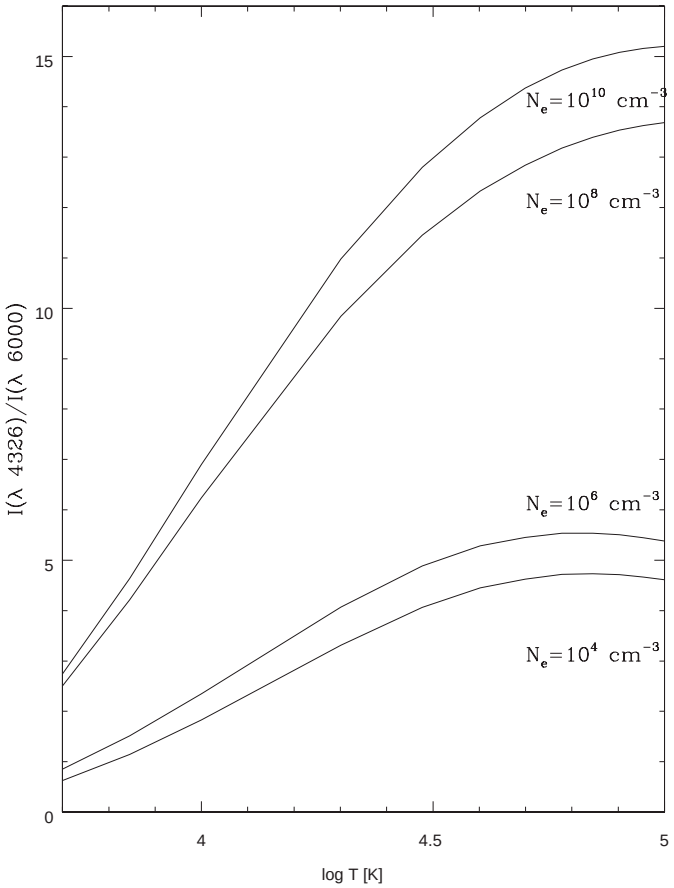

Fig. 5. λ4326 to λ6000 ratio as temperature diagnostic for different values of the electron density

References

Bautista, M. A. 1999, A&AS, 137, 529

Bautista, M. A., Peng, J., & Pradhan, A. K. 1996, ApJ, 460, 372

Berrington, K. A., Eissner, W., & Norrington, P. N. 1995, Comput. Phys. Commun., 92, 290

Dennefeld, M. 1986, A&A, 157, 267

Dennefeld, M., & Péquignot, D. 1983, A&A, 127, 42

Eissner, W., Jones, M., & Nussbaumer, H. 1974, Comput. Phys. Commun., 8, 270

Esteban, C., Peimbert, M., Torres-Peimbert, S., & Escalante, V. 1998, MNRAS, 295, 401

Fuhr, J. R., Martin, G. A., & Wiese, W. L. 1988, J. Phys. Chem. Ref. Data, 17, Suppl. 4

Garstang, R. H. 1958, MNRAS, 118, 234

Grandi, S. A. 1975, ApJ, 199, L43

Griffin, D. C., Badnell, N. R., & Pindzola, M. S. 1998, J. Phys. B: At. Mol. Opt. Phys., 31, 3713

Hass, S., Dreizler, S., Heber, U., Jeffery, S., & Werner, K. 1996, A&A, 311, 669

Henry, R. B. C., & Fesen, R. A. 1988, ApJ, 329, 693

Hudgins, D., Herter T., & Joyce, R. J. 1990, ApJ, 354, L57

Hummer, D. G., Berrington, K. A., Eissner, W., et al. 1993, A&A, 279, 298, Paper I

Johnson, D. R. H., Barlow, M. J., Drew, J. E., & Brinks, E. 1992, MNRAS, 255, 261

Oliva, E., Drapatz, S., Lutz, D., Sturm, E., & Moorwood, A. F. M. 1988, Ap&SS, 255, 2110

Osterbrock, D. E., Tran, H. D., & Veilleux, S. 1992, ApJ, 389, 305

Rudy, R. J., Rossano, G. S., & Puetter, R. C. 1994, ApJ, 426, 646

Stahl, O., & Wolf, B. 1986, A&A, 158, 371

Sugar, J., & Corliss, C. 1985, J. Phys. Chem. Ref. Data, 14 Suppl. No. 2

Watts, M. S., & Burke, V. M. 1998, J. Phys. B: At. Mol. Opt. Phys., 31, 145 (WB)